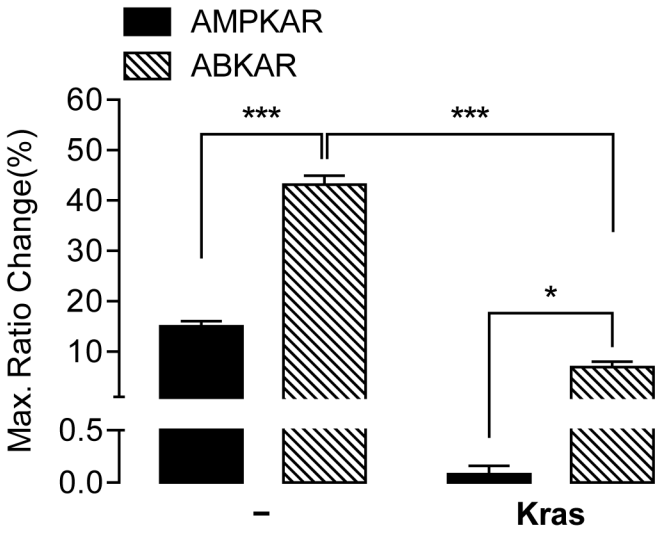

Figure S1, Related to Figure 3. Plasma membrane-localized responses from unimolecular AMPK activity biosensors. Cos7 cells were transfected with either the original AMPKAR probe or with the improved ABKAR probe containing either no localization tag (−) or a C-terminal plasma membrane-targeting sequence (Kras) and then treated with 40 mM 2DG to stimulate AMPK activity. Whereas untargeted AMPKAR displays a 15.0 ± 1.0% (n = 8) increase in the yellow-over-cyan ratio, plasma-membrane-targeted AMPKAR produces almost no response (0.1 ± 0.1%, n = 12). Furthermore, although ABKAR greatly improves on the response of AMPKAR, showing a 43.1 ± 1.8% FRET response to 2DG, plasma membrane-targeted ABKAR still exhibits a greatly diminished response in comparison (7.0 ± 1.1%, n = 15). *, $p < 0.05$; ***, $p < 0.001$ according to one-way ANOVA followed by Tukey's multiple comparisons test. Data shown represent means ± SEM.

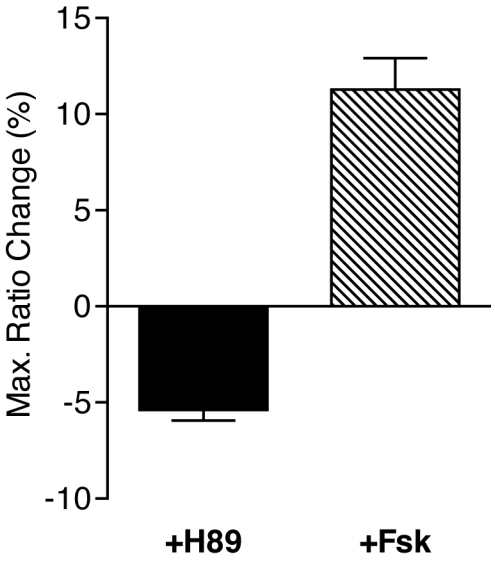

Figure S2, Related to Figure 4. Basal and stimulated PKA activity at the plasma membrane in Cos7 cells. Cos7 cells expressing AKAR4-Kras were treated with either 10 μM H89 (n = 9) or with 50 μM Fsk (n = 14). Treatment with H89 leads to a decrease in the AKAR FRET response, which is indicative of the presence of basal PKA activity, whereas treatment with Fsk treatment increases the FRET response, indicating PKA activation. Data shown represent means ± SEM.

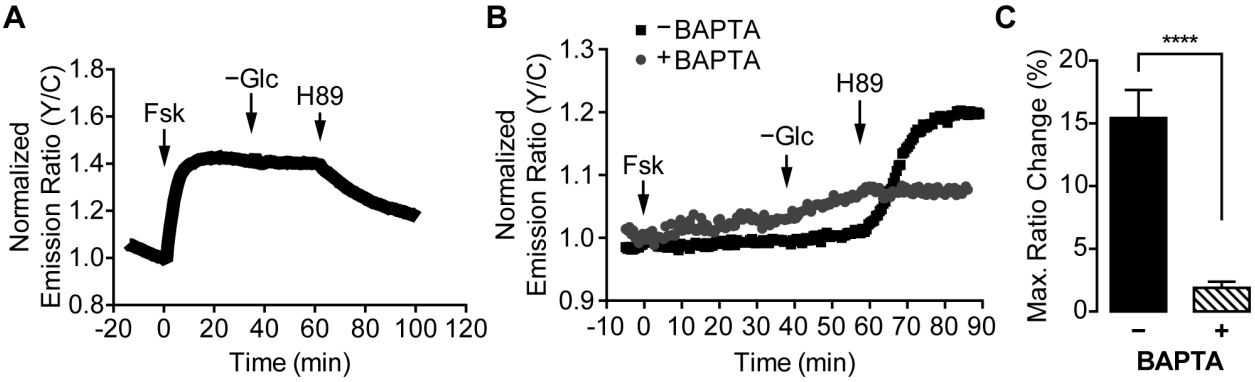

Figure S3, Related to Figure 5. (A) PKA activation and inhibition at the plasma membrane in HeLa cells. AKAR4-Kras-expressing HeLa cells were imaged in buffer containing 4.5 g/L glucose. Cells were initially stimulated with 50 μM Fsk to induce PKA activity, after which the imaging buffer was washed out and replaced with buffer lacking glucose (−Glc). Finally, cells were treated with 10 μM H89 to inhibit PKA activity. A representative single-cell trace is shown (n = 12). (B, C) PKA inhibition induces Ca^{2+}-dependent AMPK activity in HeLa cells. (B) Representative single-cell traces of HeLa cells expressing bimABKAR-Kras treated with 50 μM forskolin (Fsk), glucose deprivation (−Glc), and 10 μM H89 in the presence or absence of pretreatment with 20 μM BAPTA. (C) Bar graph summarizing the H89-induced bimABKAR-Kras FRET ratio increase in the absence (−, n = 16) and presence (+, n = 19) of 20 μM BAPTA pretreatment. ****, $p < 0.0001$ according to unpaired Student's t test. Bars represent means ± SEM.

Table S1, Related to Experimental Procedures. Summary of biosensors used in this study.

Sensor	FP (N)	**PAABD**	**Linker 1**	**Substrate**	**Linker 2**	FP (C)	Targeting
JNKAR1-NES	ECFP	FHA1	SAGKPGSGEGSTKGL	VDSVKTPEDEGNPLLEQLEKK	GGTGGS	Citrine	LPPLERLTL
bimJNKAR							
Cer-FHA-NES	Cerulean	FHA1	–	–	–	–	LPPLERLTL
JNKsub-YPet-NES	–	–	–	VDSVKTPEDEGNPLLEQLEKK	GGTGGS	YPet	LPPLERLTL
EKARcyto	Cerulean	WW	$(G)_{24}$-AR-$(G)_{24}$-AS-$(G)_{24}$	PDVPRTPVGKFQFP	PRAREI	Venus	LQKKLEELELDE
bimEKAR							
Cer-WW-NES	Cerulean	WW	–	–	–	–	LPPLERLTL
ERKsub-Ven-NES	–	–	–	PDVPRTPVGKFQFP	PRAREI	Venus	LPPLERLTL
ABKAR-NES	Cerulean3	FHA1	SAGKPGSGEGSTK	MRRVATLVDL	GTGGS	cpVenus[E172]	LPPLERLTL
bimABKAR							
Cer-FHA-NES	Cerulean	FHA1	–	–	–	–	LPPLERLTL
AMPKsub-YPet-NES	–	–	–	MRRVATLVDL	GGTGGS	YPet	LPPLERLTL
ABKAR-Kras	Cerulean3	FHA1	SAGKPGSGEGSTK	MRRATLVDL	GTGGS	cpVenus[E172]	KKKKKKSKTKCVIM
bimABKAR-Kras							
Cer-FHA-NES	Cerulean	FHA1	–	–	–		KKKKKKSKTKCVIM
AMPKsub-YPet-Kras	–	–	–	MRRVATLVDL	GGTGGS	YPet	KKKKKKSKTKCVIM

SUPPLEMENTAL EXPERIMENTAL PROCEDURES

BimKAR Construction

The PAABD-containing fragment of the bimJNKAR and bimABKAR reporters has been described previously (Herbst et al., 2011). Briefly, Cerulean-FHA1 was generated by PCR amplification and then subcloned into pcDNA3 (Invitrogen) containing a 3'-NES (LPPLERLTL) (pcDNA3-NES). The kinase-specific fragments of bimJNKAR (VDSVKTPEDEGNPLLEQLEKK) and bimABKAR (MRRVATLVDL) were PCR amplified from the respective unimolecular constructs (Fosbrink et al., 2010; Tsou et al., 2011) and subcloned into pcDNA3 containing YPet-NES. bimABKAR-Kras was subsequently generated by subcloning the AMPKsubstrate-YPet fragment into pcDNA3 containing a plasma membrane-targeting motif (KKKKKKSKTKCVIM) derived from K-Ras (Depry et al., 2011; Gao and Zhang, 2008). For bimEKAR, a fragment containing Cerulean-WW, as well as a fragment containing the Cdc25C peptide, docking domain, and Venus from unimolecular EKAR (Harvey et al., 2008), were each PCR amplified and subcloned into pcDNA3-NES. All constructs were verified by sequencing. See also Table S1.

Other Plasmids

JNKAR1 (Fosbrink et al., 2010), ABKAR (Sample et al., 2015), and AKAR4-Kras (Depry et al., 2011) have been described previously. EKARcyto (Harvey et al., 2008) and AMPKAR (Tsou et al., 2011) were gifts of Karel Svoboda (Janelia Farm Research Campus, HHMI, Ashburn, VA) and Lewis Cantley (Weill Cornell Medical College, New York, NY), respectively. AMPKAR-Kras and ABKAR-Kras were generated by subcloning AMPKAR and ABKAR, respectively, into a pcDNA3-Kras backbone. mCherry-tagged WT LKB1 and kinase-

dead LKB1-K78I (KD) were generated by subcloning the corresponding LKB1 coding sequences from pcDNA3-FLAG-LKB1 and pcDNA3-FLAG-KD LKB1 (Shaw et al., 2004) (Addgene plasmid #8590 and #8591, kindly made available by Lewis Cantley) into a pcDNA3 backbone containing the RFP variant mCherry (pcDNA3-mCherry). mCherry-LKB1-S431A, which lacks the C-terminal PKA phosphorylation site, was then generated from mCherry-LKB1 via site-directed mutagenesis. All constructs were verified by sequencing.

Reagents

Anisomycin (Sigma-Aldrich), JNK inhibitor VIII (EMD Chemicals, Darmstadt, Germany), epidermal growth factor (EGF, Sigma-Aldrich), U0126 (Sigma-Aldrich), 2-deoxyglucose (2DG), compound C (Calbiochem), forskolin (Fsk; Calbiochem), H89 (Sigma-Aldrich), and 1,2-bis(o-aminophenoxy)ethane-N,N,N',N'-tetraacetic acid acetoxymethyl ester (BAPTA-AM; Life Technologies) were used at the indicated concentrations. 2DG was prepared in HBSS. All other drugs were prepared in DMSO.

BimKAR Imaging and Analysis

For bimKAR imaging experiments, special care was taken to ensure that only cells expressing comparable amounts of both biosensor components were imaged. During transfection, plasmid DNA encoding both the N- and C-terminal bimKAR fragments was thoroughly mixed at a 1:1 ratio (typically 500 ng per construct), diluted in Opti-MEM low-serum medium (Invitrogen), and mixed with Lipofectamine 2000 diluted in Opti-MEM. Only cells that displayed clear, robust expression of both CFP and YFP were selected for imaging and subsequent analyses; cells that lacked fluorescence in either channel were excluded. Images were

analyzed in Metafluor 7.7 software (Molecular Devices, Sunnyvale, CA) by defining a region of interest (ROI) encompassing the cytoplasm of each cell in the recorded field; any nuclear fluorescence intensity was excluded. Background correction was performed in each channel by subtracting the intensity from an ROI corresponding to untransfected cells or to a cell-free region of the imaging dish. FRET ratios were calculated for each ROI by dividing the background-subtracted intensity from the FRET channel (CFP excitation, YFP emission) by the intensity from the CFP channel (CFP excitation, CFP emission) at each timepoint.

All FRET responses in this study correspond to relative changes in FRET, and no bleed-through corrections were performed. However, for more quantitative applications using bimolecular probes, it is essential to correct for spectral bleed-through into the FRET channel caused by a combination of donor (e.g., CFP) emission in the FRET channel and direct excitation of the acceptor (e.g., YFP) during donor excitation, and the literature contains several excellent examples for performing bleed-through corrections (Berney and Danuser, 2003; Chamberlain et al., 2000; Chen et al., 2007; Xia and Liu, 2001). Briefly, cells expressing only CFP are imaged in both the FRET and CFP channels to calculate a CFP bleed-through factor by dividing the background-subtracted intensity of the FRET channel by that of the CFP channel. The YFP bleed-through factor should be similarly determined by acquiring FRET and YFP images of cells expressing only YFP. CFP and YFP intensities acquired during the actual experiment are then multiplied by the corresponding correction factor, and this bleed-through signal is then subtracted from the corresponding background-subtracted FRET channel intensity.

Statistical Analysis

All statistical analyses were performed using GraphPad Prism version 5.0f (GraphPad Software, La Jolla, CA). Pairwise comparisons were performed using Student's t test, and comparisons between more than two groups were performed using one-way ANOVA followed by Tukey's multiple comparisons test to compare individual means. Statistical significance was set at $p < 0.05$. Bar graphs depict means ± SEM.

SUPPLEMENTAL REFERENCES

Berney, C., and Danuser, G. (2003). FRET or no FRET: a quantitative comparison. Biophys J *84*, 3992–4010.

Chamberlain, C.E., Kraynov, V.S., and Hahn, K.M. (2000). Imaging spatiotemporal dynamics of Rac activation in vivo with FLAIR. Meth Enzymol *325*, 389–400.

Chen, Y., Mauldin, J.P., Day, R.N., and Periasamy, A. (2007). Characterization of spectral FRET imaging microscopy for monitoring nuclear protein interactions. J Microsc *228*, 139–152.

Depry, C., Allen, M.D., and Zhang, J. (2011). Visualization of PKA activity in plasma membrane microdomains. Mol Biosyst *7*, 52.

Fosbrink, M., Aye-Han, N.N., Cheong, R., Levchenko, A., and Zhang, J. (2010). Visualization of JNK activity dynamics with a genetically encoded fluorescent biosensor. Proc Natl Acad Sci USA *107*, 5459–5464.

Gao, X., and Zhang, J. (2008). Spatiotemporal analysis of differential Akt regulation in plasma membrane microdomains. Mol Biol Cell *19*, 4366–4373.

Harvey, C.D., Ehrhardt, A.G., Cellurale, C., Zhong, H., Yasuda, R., Davis, R.J., and Svoboda, K. (2008). A genetically encoded fluorescent sensor of ERK activity. Proc Natl Acad Sci USA *105*, 19264–19269.

Herbst, K.J., Allen, M.D., and Zhang, J. (2011). Luminescent kinase activity biosensors based on a versatile bimolecular switch. J Am Chem Soc *133*, 5676–5679.

Sample, V., Ramamurthy, S., Gorshkov, K., Ronnett, G.V., and Zhang, J. (2015). Polarized Activities of AMPK and BRSK in Primary Hippocampal Neurons. Mol Biol Cell.

Shaw, R.J., Kosmatka, M., Bardeesy, N., Hurley, R.L., Witters, L.A., DePinho, R.A., and Cantley, L.C. (2004). The tumor suppressor LKB1 kinase directly activates AMP-activated kinase and regulates apoptosis in response to energy stress. Proc Natl Acad Sci USA *101*, 3329–3335.

Tsou, P., Zheng, B., Hsu, C.-H., Sasaki, A.T., and Cantley, L.C. (2011). A fluorescent reporter of AMPK activity and cellular energy stress. Cell Metabolism *13*, 476–486.

Xia, Z., and Liu, Y. (2001). Reliable and global measurement of fluorescence resonance energy transfer using fluorescence microscopes. Biophys J *81*, 2395–2402.